

Effect of Slip Zone Structure on Earthquake Rupture Velocity

G. G. Kocharyan^{1*}, A. M. Budkov¹, and S. B. Kishkina¹

¹ *Sadovsky Institute for Dynamics of Geospheres, Russian Academy of Sciences, Moscow, 119334 Russia*

* *e-mail: gevorgkidg@mail.ru*

Received May 14, 2022; revised June 24, 2022; accepted June 24, 2022

Abstract—The paper presents a brief analysis of the accumulated data on fast dynamics of earthquake ruptures and their qualitative comparison with the numerical results on supershear rupture propagation along homogeneous and heterogeneous fault surfaces. Calculation methods and parameters are described. The numerical results indicate that the rupture velocity in strong earthquakes can vary in a wide range, exceeding significantly the Rayleigh wave velocity treated as the maximum possible crack velocity in conventional fracture mechanics. It is shown that a necessary condition for the transition to supershear rupture propagation along the heterogeneous contact surface is the presence of a sufficient number of asperity contact spots that experience rapid frictional weakening during shear. The rupture velocity can periodically decrease or increase in the case of a heterogeneous fracture surface. Systematic variation in fault properties along strike increases the probability of supershear rupture in old contact segments.

Keywords: earthquake source, fault, slip regimes, rupture velocity, supershear rupture, numerical simulation, frictional behavior, surface roughness

DOI: 10.1134/S1029959922060078

1. INTRODUCTION

For the 25 years of existence of the *Physical Mesomechanics* journal, its authors repeatedly addressed the problems of fault zone mechanics [1, 2, etc.]. Faults, these fascinating natural objects, are a typical example of a hierarchically organized complex system, with various mechanical interactions, physico-chemical and metamorphic transformations occurring in them. The presence of faults ensures the mobility of the Earth's crust, its permeability to fluids, and determines most evolution processes in the upper and middle crust. The first editor-in-chief V.E. Panin perceived the importance of physical mesomechanics in describing these processes and included (along with strength physics, materials science, fracture mechanics, etc.) geomechanics and geodynamics into the scope of the journal.

Since the first experimental measurements of earthquake rupture velocity in the 50–60s of the last century, the maximum rupture velocity has been thought to be close to the Rayleigh wave velocity C_R , which is the maximum possible crack velocity in conventional analytical models of fracture mechanics

[3]. In most cases, the average earthquake rupture velocity V_r falls within the range from 1100 to 3100 m/s, which corresponds to the classical concepts [4].

Increasing attention of contemporary geophysicists and mechanics is given to the fact that ruptures in certain earthquakes can periodically have an unusually high velocity (above the C_R value). The crack velocity exceeding the shear wave velocity C_s was first recorded in the early 1970s, in laboratory experiments on plastic polymer [5]. Shortly afterwards it was analytically and numerically shown that a stress concentration zone propagates ahead of the primary crack front at the velocity C_s with friction but without cohesion [6, 7]. In so doing, the stress peak gradually increases until it overcomes the local strength of the fault. This results in the so-called “daughter crack”, which is initially insulated from the main fault. The leading front of the daughter crack starts as an unstable supershear rupture, which rapidly accelerates and transforms into a stable supershear rupture. The trailing front quickly merges with the main fault, placing the entire crack in the supershear regime. The condi-

tion for supershear rupture is the shear-induced weakening of the contact surface and a sufficient level of background stresses [7].

The reasons for the formation of this stress concentration zone are still unclear. In [8], it was related to an elastic vortex that rapidly propagates in front of the crack. In [9], a supershear rupture was explained by the presence of a more rigid inclusion in the crack path, which can directly lead to dynamic stress concentrations and localized instability.

Although seismologists were initially skeptical about these results, theoretical works stimulated a search for real supershear ruptures. In the early 2000s, the results of field observations during several earthquakes finally confirmed that in some cases, as a rule, in some fault segments, the rupture velocity reaches anomalously high values [4, 10, and their references].

This phenomenon is not only of fundamental (for crack theory) but also of clear practical significance (including for engineering seismology). The amplitude of the ground motion in the shear wave group at the emerging plane fronts, similar to Mach fronts, attenuates much more slowly than that of “normal” sub-Rayleigh ruptures [10]. This can lead to a noticeable increase in the earthquake intensity both in the vicinity of the rupture and at significant distance from the epicenter.

Though the main mechanisms of intersonic crack propagation are understood, the role of structural heterogeneity of the slip surface has not yet been adequately investigated. The aim of this paper is to elucidate the influence of the slip zone structure on the slip evolution. To do this, we perform a brief analysis of the accumulated data on the fast dynamics of earthquake ruptures and their qualitative comparison with the numerical results on supershear rupture propagation along homogeneous and heterogeneous fault surfaces.

2. SOME OBSERVATIONAL RESULTS

In most cases, the rupture velocity is estimated from the low-frequency data of teleseismic observations, providing only the average rupture velocity during the process in the epicenter. Though the accuracy of the V_r measurement is rather low, the main trends can be determined quite reliably. Thus, the authors of [4] analyzed the data on 96 earthquakes with the magnitude M_w from 6.4 to 8.1 and found that about 25% of them has the average rupture velocity in the range from 3100 to 4500 m/s.

Table 1. Average and maximum rupture velocities in certain earthquakes

Event	$V_{r\max}$, km/s	\hat{V}_r , km/s	C_s , km/s
M7.8 Kunlun, 11.11.2001	4.83–5.52	3.31–3.67	3.50
M7.5 Indonesia, 10.10.2002		3.15–3.34	3.70
M7.8 Denali, 03.11.2002	4.94–5.58	3.11–3.39	3.50
M7.5 Carlsberg Ridge, 15.07.2003		3.47–3.95	4.65
M8.6 Sumatra, 11.04.2012	4.90–6.07	4.14–4.94	4.65
M8.2 Sumatra, 1.04.2012	5.00–6.20	3.30–4.50	4.65
M7.5 Alaska, 05.01.2002		2.91–3.76	3.70
M7.7 Pakistan, 24.09.2013	4.99–6.55	4.15–4.98	3.60

The analysis of high-frequency near-field records (for example, [11]) increases chances to discover features of the rupture process. Good results come from the method of inversion of seismic data from several dense seismic networks, yielding accurate estimates of the arrival time of high-frequency longitudinal waves emitted by each fault segment (for example, [12]). It was noted that superfast ruptures are characteristic mainly of strike-slip faults. The authors of [12] analyzed the data on 15 dip-slip faults of large earthquakes and 8 strike-slip faults with a shallow-depth source. Five of the eight strike-slip faults had a much higher maximum rupture velocity $V_{r\max}$ than C_s , while their average \hat{V}_r corresponded to the sub-Rayleigh regime. At the same time, the supershear regime was found in none of the 15 dip-slip events. Data on the eight earthquakes are given in Table 1.

Many earthquakes, including supershear ones, are characterized by low values of V_r at the initial stage. Figure 1a shows a schematic of the rupture propagation of the well-known 2002 M_w 7.9 Denali earthquake in Alaska. The rupture started along the 40-km segment of the Susitna Glacier thrust fault. Then it arrived at the Denali strike-slip fault system and followed the main Denali fault for 218 km from west to east. Thereafter the rupture branched and turned to the Totchunda fault, staying on its trace for another 76 km to a stop [13]. The data on the rupture velocity of this earthquake are somewhat different. The supershear segment was first found to be 38 km in length

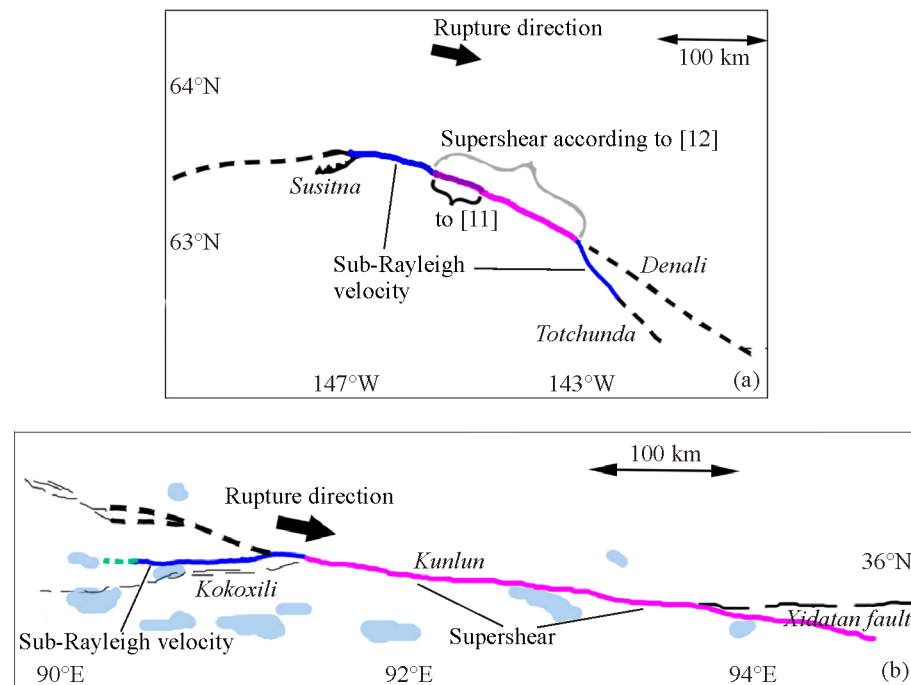


Fig. 1. Schematic of ruptures in 2002 M_w 7.9 Denali earthquake, Alaska (a) and 2001 M_w 7.8 Kunlun, China (b) (color online).

[11]. However, according to the later paper [12], the rupture kept a high velocity V_r until it intersected the Totchunda fault (Fig. 1a), decelerating sharply afterwards.

Another example is the 2001 M_w 7.8 Kunlun earthquake in China [14] (Fig. 1b). This rupture was initiated at the westernmost end of the secondary fault and propagated at a rather low velocity for the first 20–30 km, advancing eastward for 20–30 s. Then the rupture followed the main Kunlun fault for another ~400 km, changing its slope angle by almost 20°. In [14], the rupture velocity was calculated to be $V_r \sim 3.3 \text{ km/s} \sim 0.94C_s$ for the first 120 km. Then, it reached more than 6 km/s, exceeding periodically C_p . The seismic inversion method gives more stable values $V_r \sim 4.83\text{--}5.22 \text{ km/s}$ for this segment [12]. Moreover, maximum displacement was recorded in the same fault segment.

In [15], the authors analyzed the location of fault segments with maximum coseismic displacements and with high rupture velocities using data on 27 large ($M_w \geq 6.5$) continental earthquakes. The data analysis was performed with careful geological interpretation. Consideration was given to the fault age, direction of long-term fault propagation, and other data. The authors found that large displacement amplitudes and maximum rupture velocities are most likely to appear in the mature fault, which is remote from its leading, geologically the youngest, end.

These effects are supposedly induced by the along-strike heterogeneity of fault properties formed during geological evolution [15].

In terms of physical mesomechanics, three levels of heterogeneity should be distinguished.

At the macrolevel, the heterogeneity manifests itself as a systematic along-strike variation in fault properties. In the case of a one-sided fault, this concerns the properties both of the central part containing the fault core and the slip zone and of the damage zone. The stiffness and effective strength of the material of the slip zone decrease from the fault end (conditional crack tip) to its geological origin. In addition, many kilometers of slip make macroasperities more and more flat and gentle [16]. While the initial stages of fault evolution are characterized by intensive fragmentation of asperities, mature faults slip with friction along flattened asperities, i.e. the slip surface becomes smoother. On the one hand, this enlarges the segments with friction weakening properties, and on the other hand, their effective strength is likely to decrease as compared to the young segments, which is due to a decrease in the concentration of normal stresses at asperities.

The mesoscopic heterogeneity is revealed in local areas of the contact surface that explicitly exhibit weakening properties at higher slip velocity and/or amplitude. Most likely these areas represent more or less dense clusters of asperities of the lower level and

are usually located unevenly on the fault plane. Since weakening is one of the most important conditions of earthquake generation, these areas can be taken as concentrations of hypocenters of low-magnitude earthquakes. Such clusters comprise the main “friction element”, which determines the integral features of fault shear resistance. Hypocenters of larger events are often located in the vicinity of the boundaries of these areas [17].

Judging from the results of field studies on slip zones [16], shear deformation is highly localized during slip. Seismogenic slip often occurs in the ultracataclastic, clay-bearing zone tens to hundreds of millimeters thick (fault core), but the principle coseismic slip can be localized in a zone thinner than 1–5 mm inside this ultracataclastic core. In this regard, the macroscopic effects of friction are largely determined by processes occurring at the microlevel. On the scale 0.01–10 μm , the fault friction is reduced primarily by wear (decrease in roughness), while the roughness on large scales of natural faults has a limited effect on the basic friction coefficient [18].

The role of macro- and mesoheterogeneity in strike-slip faulting will be numerically studied in the next section.

3. PROCEDURE

The problem of faulting at the boundary of two homogeneous elastic blocks was solved by numerical mathematical modeling. Use was made of a two-dimensional software package [19] based on the Lagrangian numerical method called Tensor. Calculations were performed in a two-dimensional formulation. A system consisting of two elastic blocks was considered. The Cartesian axes lay in the contact plane (axis X) and perpendicular to it (axis Y). The field of uniform shear stresses $\sigma_{xy} = \tau_0$ was set as the initial condition. The heterogeneity of frictional properties on the slip surface was modeled by alternating friction weakening (FW) zones with friction stable (FS) zones with a constant shear resistance equal to the background stress $\tau = \tau_0$. This is a typical situation under various tectonic conditions, when, during the interseismic period, active areas (asperities) are locked and do not move, while passive areas are in the state of slow creep [16].

Friction in the FW zones was given by the relation

$$\tau(u) = T(u) \operatorname{sgn}\left(\frac{\partial u}{\partial t}\right), \quad \frac{\partial u}{\partial t} \neq 0, \quad (1)$$

where

$$T(u) = \begin{cases} \tau_u - \frac{(\tau_u - \tau_f)u}{d_0}, & u < d_0, \\ \tau_f, & u \geq d_0, \end{cases}$$

u is the relative displacement of the fault walls, τ_u is the ultimate frictional strength, τ_f is the residual frictional strength, d_0 is the amplitude of a displacement during which the frictional strength decreases from the peak to residual value. During the slip process, interfacial shear stresses are always equal to τ_f .

Length normalization is performed using the Griffith critical crack half-length [7]

$$L_c = \frac{8 \mu(\lambda + \mu)}{\pi \lambda + 2\mu} \frac{G}{(\tau_0 - \tau_f)^2}.$$

Here λ and μ are the Lamé coefficients, $G = 1/4(\tau_u - \tau_f)d_0$ is the effective crack propagation energy, and τ_0 is the background shear stress.

The following model parameters are used: the density $\rho_0 = 2.5 \times 10^3 \text{ kg/m}^3$, Poisson's ratio $\nu = 0.25$, longitudinal wave velocity $C_p = 6000 \text{ m/s}$, shear wave velocity $C_s = 3460 \text{ m/s}$, $\tau_u = 16 \text{ MPa}$, $\tau_f = 5 \text{ MPa}$, and $d_0 = 1.8 \text{ mm}$. The τ_0 value can vary in different series of calculations. Hereinafter, all characteristic dimensions will be given in units L_c ($\hat{L} = L/L_c$), and time will be normalized as $\hat{t} = tC_s/L_c$. The normalized physical dimensions of the computational domain $\hat{\Sigma}$ range from 120×120 to 180×180 . The uniform computational grid consists of cells of the size $\hat{l} = 0.015 \times 0.015$.

To activate the crack propagation in a small region of the contact surface $0 \leq x \leq L_0$, we initiate a stress relief with the velocity $V_{r0} = 0.6C_s$. To do this, at each computational node x_i of the initiation region at the time instant $t_i = x_i/V_{r0}$, we set the displacement $u = 1.1u_0$, where u_0 is the threshold displacement, at which friction reaches the level of background shear stresses τ_0 of rocks: $\tau(u_0) = \tau_0$. The calculations show that the stress relief region should have a sufficient size. At $\hat{L}_0 \leq 3$, the rupture formation process dies out in the immediate vicinity of the initiation site. The parameter L_0 varies within $\hat{L}_0 = 3\text{--}6$ in the calculations.

The stress state of the contact surface is conveniently characterized by the dimensionless parameter of fault strength

$$S = \frac{\tau_u - \tau_0}{\tau_0 - \tau_f}. \quad (2)$$

It was shown in [7] that the transition to super-shear rupture propagation can occur at $S < 1.77$. From

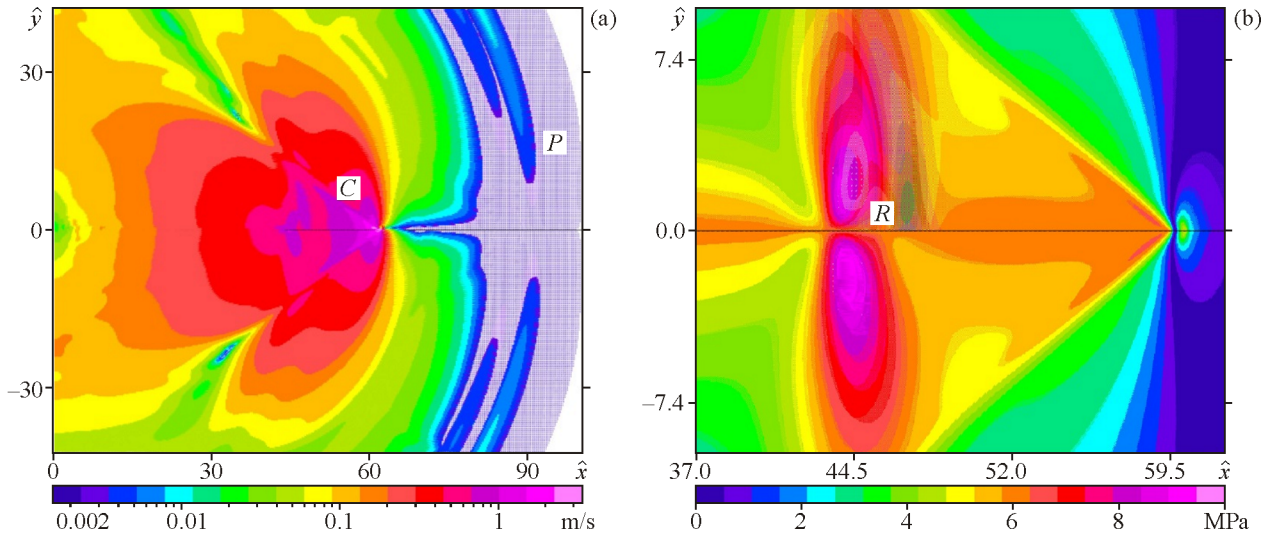


Fig. 2. Velocity vector field (a) and spatial distribution of shear stresses σ_{xy} (b) in the supershear regime ($t=56.4$) at $S=0.8$ (color online).

(2) it is easily seen that a more “brittle” fault (with a low ratio τ_f/τ_u) is characterized by lower average stresses (smaller parameter τ_0/τ_u) of transition to supershear rupture propagation.

4. CALCULATION RESULTS

The calculation results for the homogeneous contact surface (friction over the entire surface is described by relation (1)) are detailed in [20, 21]. The results obtained are in good agreement with the theoretical concepts and the previous numerical results [7, 8]. Thus, calculations with the parameter $S > 1.8$ demonstrated the wave pattern typical of the usual sub-Rayleigh regime. In this case, the displacement velocity component normal to the fault plane prevails. The rupture velocity at the initial stage approximates the velocity in the initiation region ($v_r = 0.6C_s$) and gradually increases with distance, reaching the Rayleigh wave velocity.

At $S < 1.77$, the rupture velocity grows gradually after the initiation region ($v_r = 0.6C_s$). At the distance $\hat{x} \approx 18$, the mass velocity peaks ahead of the shear wave front. After the distance $\hat{x} \approx 30$, a supershear rupture is finally formed. A longitudinal wave runs first, followed by a complex oscillation with the characteristic phase shift of the fault-tangential and fault-normal velocity components. In general, the deformation field in the supershear segment reveals an increase in the amplitude ratio between the tangential and normal displacement velocity components with

distance, i.e. the predominant displacement of the material along the fault.

We emphasize that, according to the used friction model, differential motion along the fault is initiated under the condition

$$\sigma_{xy} \geq \tau_u = \tau_0 + \Delta\tau. \quad (3)$$

The stress wave amplitude at the longitudinal wave front, as a rule, is insufficient for this condition to be fulfilled, and therefore no slip occurs along the fault. In the sub-Rayleigh regime, condition (3) is satisfied only at the shear wave front. The moment of fulfillment of condition (3) is called the initiation time of differential motion. It is at this moment that the rupture is initiated. However, the rupture begins to radiate elastic energy when the amplitude of differential displacement along the fault u exceeds the threshold displacement u_0 , at which the friction value decreases to the background stress τ_0 . This stage, referred to as active, is formed behind the shear wave front. The displacement velocity field shown in Fig. 2a at the time instant $\hat{t} = 56.4$ illustrates the ground motion in the supershear regime. The rupture propagating at the velocity of longitudinal waves moves ahead of the shear wave front. The resulting secondary shear waves form a conical wave front due to interference, the position of which in Fig. 2a is marked with the letter C. The supershear crack propagation at the initial stage is accompanied by a constant increase in the maximum velocity of rupture-induced ground displacement. At the time $\hat{t} = 56.4$, the

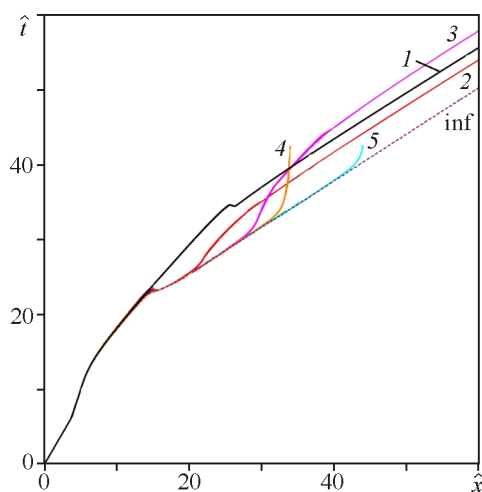


Fig. 3. Hodographs of the beginning of the active slip stage at different lengths of the FS zone starting at the point $\hat{x} = 14.8$: $\Delta\hat{x} = 0$ (1), 7.4 (2), 14.8 (3), 18.5 (4), 29.6 (5); curve inf is plotted for the case of stable friction over the entire surface (color online).

maximum displacement velocity in the active fault zone already exceeds 2 m/s.

In Fig. 2b, a small elliptical zone with increased shear stresses is seen in the vicinity of the fracture front, which is associated with the characteristic vortex motion in the medium. The highest shear stress in this zone is ~ 5 MPa, which exceeds the threshold of the onset of differential motion $\Delta\tau = 4.9$ MPa, i.e. the relative displacement of the fault walls begins in the vortex zone. A similar result was demonstrated earlier [8]. The zone of maximum shear stresses R falls behind and is formed due to the surface wave propagation, where the relative displacement of the walls chiefly accumulates (the main crack zone).

Calculations for the heterogeneous contact surface are performed in the presence of one or several “passive” zones with stable friction on it. The length of these zones varies from $\Delta\hat{x} = 3.7$ to the full length of the block. In all variants, the heterogeneous zone starts from the coordinate $\hat{x} = 14.8$. Some results of such calculations are shown in Figs. 3–5.

A rupture propagates differently through friction weakening and friction stable zones of the contact surface. As mentioned above, the amplitude of a weak longitudinal wave is not enough to move locked FW zones (asperities). At the same time, in FS zones where, at $\tau \geq \tau_0$, friction is always fully mobilized and slip acceleration induces no additional frictional strength, the differential motion of the walls propagates exactly at the velocity of the longitudinal wave. Thus, a weak longitudinal wave with the intensity in-

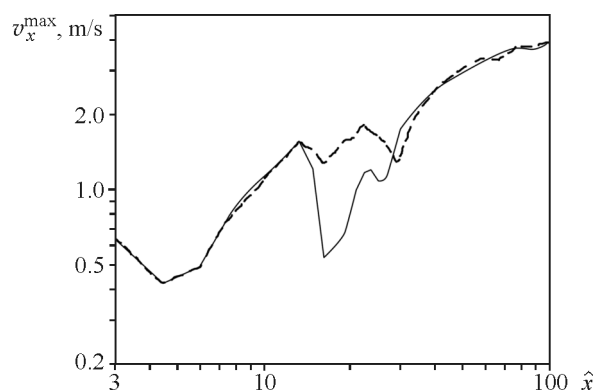


Fig. 4. Spatial distribution of the amplitude of the horizontal velocity component in the case of a homogeneous contact surface (dashed line) and in the presence of a FS zone in the segment $\hat{x} = 14.8$ –18.4 (solid line).

sufficient to move the locked FW zones (asperities) causes slip in friction stable zones. This leads to an interesting effect: the differential motion in passive FS zones starts earlier than at locked asperities. This effect explains the negative slope of the hodograph curve of the beginning of the active stage in some short segments.

If a rupture is initiated on the homogeneous FW surface without FS zones, a crack propagates any random distance (Fig. 3, curve inf).

If the FS zone is large ($\Delta\hat{x} \geq 18.5$), the rupture is arrested. The rupture propagation through the FS zone is not accompanied by the release of elastic energy stored in the block, and, consequently, the seismic wave that initiates the rupture gradually decays. If the rupture meets another FW zone with a higher frictional strength, the intensity of dynamic stresses

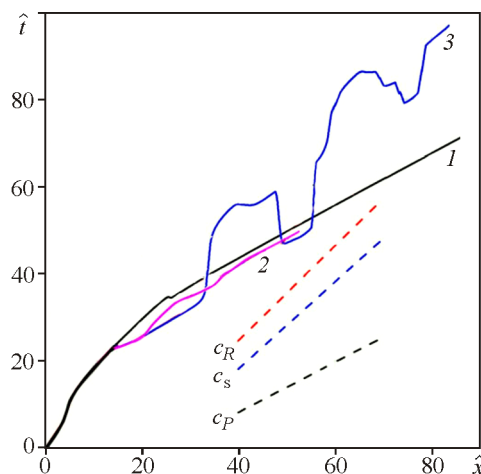


Fig. 5. Hodographs of the beginning of the active slip stage for heterogeneous surfaces with different parameters $\delta = \Delta x / L_{asp} = 0$ (1), 1.0 (2), 2.5 (3) (color online).

may be insufficient and the rupture stops (Fig. 3, curves 4 and 5). This is the only mechanism for rupture arrest within the used model.

When the surface is composed of FW zones of length L_{asp} alternating with FS zones of length Δx , the pattern of rupture propagation becomes more complicated. Figure 4 compares the distribution of the maximum amplitude of the horizontal slip velocity component over the homogeneous contact surface and the surface with a FS zone. A sharp local decrease is seen in the slip velocity amplitude in the “passive” FS zone (Fig. 4). If the passive zone is sufficiently long (more than $\Delta \hat{x} \geq 18.5$ at $S=0.8$), the rupture is arrested. Otherwise, the differential velocity amplitude is restored in the subsequent active FW zone. Then the transition of the sub-Rayleigh rupture to the supershear regime begins. On the heterogeneous interface, such drops in the shear amplitude occur near each FS zone.

The hodographs of the beginning of the active slip stage for several heterogeneous surfaces are shown in Fig. 5. The length of each FW zone is $\hat{L}_{asp} = L_{asp}/L_c \approx 7.4$. The parameter $\delta = \Delta x/L_{asp}$ characterizing the density of active FW zones (asperities) varies in calculations from 0 to 2.5. This means that, the larger the parameter δ , the smaller the area occupied by FW zones.

If FS zones become longer, the transition to the supershear regime occurs farther and farther from the site where the heterogeneity begins. At $\delta \geq 1.0$, the pattern is complicated by special features in transition zones, but in the end the crack velocity exceeded the C_s value in all cases, except for $\delta=2.5$. At the parameter $\delta=2.5$ (the fraction of FW zones is less than 30%), the rupture is arrested.

5. CONCLUSIONS

The observational analysis and the performed numerical calculations showed a very wide range of rupture velocities in strong earthquakes. This conclusion is of importance in engineering seismology as well as for a fundamental understanding of earthquake source mechanics.

A necessary condition for the transition to supershear rupture propagation along the heterogeneous contact surface is the presence of a sufficient number of asperity contact spots, which experience rapid frictional weakening during shear. At the same time, the more “brittle” the asperity (the lower the residual frictional strength as compared to the peak value), the lower the average stresses of transition to super-

shear rupture. The higher microroughness of the contact surface increases the frictional “brittleness” of the asperity, thereby enhancing the probability of initiating a supershear rupture.

The mesoscopic heterogeneity makes the wave pattern more difficult: there appear intervals of decrease and increase in rupture velocity and coseismic displacement amplitude. After arriving at a long FS zone, the supershear rupture continues to propagate at a velocity of the longitudinal wave, although the amplitude of the differential motion decays. Ultimately, the rupture is arrested when it meets a locked zone, which can not be already destroyed at the dynamic impact amplitude.

Macroscopic heterogeneities—systematic along-strike variation in fault properties—increase the probability of fast ruptures in old fault segments.

The calculation results on a simple model do not contradict the seismological data, reflecting such phenomena as a gradual increase in rupture velocity, rupture acceleration and deceleration, a higher probability of supershear ruptures in worn-in fault segments with flatter, wider asperities, long-range propagation of a supershear rupture, and its sudden arrest.

Thus, the calculation results showed that a fast rupture is more likely to occur in rough (wavy) areas of the contact surface, in which contact spots are closely spaced. The propagation of such a rupture with the attenuating displacement amplitude can be stable in locally smoother areas. A similar result was obtained in [22].

FUNDING

This work was supported by the Russian Science Foundation (project No. 22-27-00565).

REFERENCES

1. Kostyuchenko, V.N., Kocharyan, G.G., and Pavlov, D.V., Strain Characteristics of Interblock Gaps of Different Scales, *Phys. Mesomech.*, 2002, vol. 5, no. 5–6, p. 21–38.
2. Psakhie, S.G., Ruzhich V.V., Smekalin, O.P., and Shilko, E.V., Response of the Geological Media to Dynamic Loading, *Phys. Mesomech.*, 2001, vol. 4, no. 1, p. 63–66.
3. Kostrov, B.V. and Shamita Das, *Principles of Earthquake Source Mechanics*, Cambridge: Cambridge University Press, 1989.
4. Chouneta, A., Valléa, M., Causseb, M., and Courboux, F., Global Catalog of Earthquake Rupture Velocities Shows Anticorrelation between Stress Drop

- and Rupture Velocity, *Tectonophysics*, 2018, vol. 733, no. 9, pp. 148–158. <https://doi.org/10.1016/j.tecto.2017.11.005>
5. Wu, F.T., Thomson, K., and Kuenzler, H., Stick-Slip Propagation Velocity and Seismic Source Mechanism, *Bull. Seism. Soc. Am.*, 1972, vol. 62, pp. 1621–1628.
 6. Burridge, R., Admissible Speeds for Plane-Strain Self-Similar Shear Cracks with Friction But Lacking Cohesion, *J. R. Astr. Soc.*, 1973, vol. 35, p. 439.
 7. Andrews, D.J., Rupture Velocity for Plane Strain Shear Cracks, *J. Geophys. Res.*, 1976, vol. 81, p. 5679.
 8. Psakhie, S.G., Shilko, E.V., Popov, M.V., and Popov, V.L., Key Role of Elastic Vortices in the Initiation of Intersonic Shear Cracks, *Phys. Rev. E*, 2015, vol. 91, p. 063302. <https://doi.org/10.1103/PhysRevE.91.063302>
 9. Stefanov, Yu.P., Initiation and Propagation of Rupture in the Fault Zone, *Fiz. Mezomekh.*, 2008, vol. 11, no. 1, pp. 94–100.
 10. Das, S., Supershear Earthquake Ruptures—Theory, Methods, Laboratory Experiments and Fault Superhighways: An Update, in *Perspectives on European Earthquake Engineering and Seismology*, Ansal, A., Ed., Springer, 2015, pp. 1–20. https://doi.org/10.1007/978-3-319-16964-4_1
 11. Ellsworth, W.L., Celebi, M., Evans, J.R., Jensen, E.G., Kayen, R., Metz, M.C., Nyman, D.J., Roddick, J.W., Spudich, P., and Stephens, C.D., Near-Field Ground Motion of the 2002 Denali Fault, Alaska, Earthquake Recorded at Pump Station 10, *Earthq. Spectra*, 2004, vol. 20, pp. 597–615. <https://doi.org/10.1193/1.1778172>
 12. Wang, D.D., Mori, J., and Koketsu, K., Fast Rupture Propagation for Large Strike-Slip Earthquakes, *Earth Planetary Sci. Lett.*, 2016, vol. 440, pp. 115–126. <https://doi.org/10.1016/j.epsl.2016.02.022>
 13. Haeussler, P.J., Schwartz, D.P., Dawson, T.E., Stenner, H.D., Lienkaemper, J.J., Sherrod, B., Cinti, F.R., Montone, P., Craw, P.A., Crone, A.J., and Personius, S.F., Surface Rupture and Slip Distribution of the Denali and Totschunda Faults in the 3 November 2002 M7.9 Earthquake, Alaska, *Bullet. Seismol. Soc. Am. B*, 2004, vol. 94, no. 6, pp. S23–S52.
 14. Robinson, D.P., Brough, C., and Das, S., The Mw 7.8, 2001 Kunlunshan Earthquake: Extreme Rupture Speed Variability and Effect of Fault Geometry, *J. Geophys. Res. B*, 2006, vol. 111, p. 08303. <https://doi.org/10.1029/2005JB004137>, <https://www.researchgate.net/publication/241924204>
 15. Perrin, C., Manighetti, I., Ampuero, J.P., Cappa, F., and Gaudemer, Y., Location of Largest Earthquake Slip and Fast Rupture Controlled by Along-Strike Change in Fault Structural Maturity due to Fault Growth, *J. Geophys. Res.*, 2016, vol. 121, no. 5, pp. 3666–3685. <https://doi.org/10.1002/2015JB012671>
 16. Kocharyan, G.G. and Kishkina, S.B., The Physical Mesomechanics of the Earthquake Source, *Phys. Mesomech.*, 2021, vol. 24, no. 4, pp. 343–356. <https://doi.org/10.1134/S1029959921040019>
 17. Ostapchuk, A., Polyatykin, V., Popov, M., and Kocharyan, G., Seismogenic Patches in a Tectonic Fault Interface, *Front. Earth Sci.*, 2022. <https://doi.org/10.3389/feart.2022.904814>
 18. Chen, X., Madden, A.S., Bickmore, B.R., and Reches, Z., Dynamic Weakening by Nanoscale Smoothing during High-Velocity Fault Slip, *Geology*, 2013, vol. 41, no. 7, pp. 739–742. <https://doi.org/10.1130/G34169.1>
 19. Arkhipov, V.N., Borisov, V.A., Budkov, A.M., Val'ko, V.V., Galiev, A.M., Goncharova, O.P., Zaikov, I.M., Zamyshlyayev B.V., Knestyapin, A.M., Korolev, V.S., Kuzovlev, V.D., Makarov, V.E., Seliverstov, I.Yu., Semenov, G.I., Smaznov, V.V., Smirnov, E.I., and Ushakov, O.N., *Mechanical Effect of Nuclear Explosions*, Moscow: Fizmatlit, 2003.
 20. Budkov, A.M. and Kocharyan, G.G., Numerical Modeling of the Supershear Rupture Propagation along the Homogeneous and Heterogeneous Fault Surfaces, *Dinam. Prots. Geosf.*, 2021, no. 13, pp. 10–19
 21. Budkov, A.M., Kishkina, S.B., and Kocharyan, G.G., Modeling Supershear Rupture Propagation on a Fault with Heterogeneous Surface, *Izv. Phys. Sol. Earth*, 2022, vol. 58, no. 4, pp. 562–575.
 22. Bruhat, L., Fang, Z., and Dunham, E.M., Rupture Complexity and the Supershear Transition on Rough Faults, *J. Geophys. Res. Solid Earth*, 2016, vol. 121, pp. 210–224. <https://doi.org/10.1002/2015JB012512>